ACS Catalysis

Research Article

pubs.acs.org/acscatalysis

Nonheme Iron Oxidant Formed in the Presence of H_2O_2 and Acetic Acid Is the Cyclic Ferric Peracetate Complex, Not a Perferryloxo Complex

Yong Wang,*[,†] Deepa Janardanan,[‡] Dandamudi Usharani,[‡] Keli Han,[†] Lawrence Que, Jr.,*[,§] and Sason Shaik*[,‡]

[†]State Key Laboratory of Molecular Reaction Dynamics, Dalian Institute of Chemical Physics, Chinese Academy of Sciences, Dalian 116023, China

[‡]The Institute of Chemistry and the Lise Meitner-Minerva Center for Computational Quantum Chemistry, The Hebrew University of Jerusalem, Jerusalem 91904, Israel

[§]Department of Chemistry and the Center for Metals in Biocatalysis, University of Minnesota, Minneapolis, Minnesota 55455, United States

Supporting Information

ABSTRACT: Oxidative C−H bond activation is a transformation of fundamental and practical interest, particularly if it can be carried out with high regio- and enantioselectivity. With nonheme iron oxygenases as inspiration (e.g., the Rieske oxygenases), a family of biomimetic nonheme iron complexes has been found to catalyze hydrocarbon oxidations by H_2O_2 via a postulated $Fe^{V}(O)(OH)$ oxidant. Of particular interest is the Fe(*S*,*S*-PDP) catalyst discovered by White that, in the presence of acetic acid as an additive, performs selective C−H bond activation, even in complex organic molecules. The corresponding $Fe^{V}(O)(OAc)$ species has been suggested as the key oxidant. We have carried out DFT studies to assess the viability of such an oxidant and discovered an alternative formulation. Theory reveals that the barrier for the formation of the putative $Fe^{V}(O)(OAc)$ oxidant is too high for it to be feasible. Instead, a much lower barrier is found for the formation of a $[(S,S\text{-PDP})Fe^{III}(\kappa^2\text{-peracetate})]$ species. In the course of C−H activation, this complex undergoes O−O bond homolysis to become a transient $[(S,S\text{-PDP})Fe^{IV}(O)(AcO\cdot)]$ species that performs the efficient hydroxylation of alkanes. Thus, the acetic acid additive alters completely the nature of the high-valent oxidant, which remains disguised in the cyclic structure. This new mechanism can rationalize the many experimental observations associated with the oxidant formed in the presence of acetic acid, including the $S = 1/2$ EPR signal associated with the oxidant. These results further underscore the rich multioxidant scenario found in the mechanistic landscape for nonheme iron catalysts.

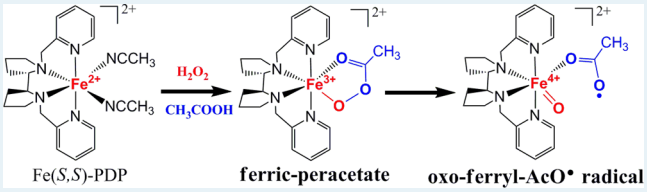

KEYWORDS: *nonheme iron, C−H activation, density functional calculations, oxometal, O−O homolysis*

INTRODUCTION

Oxidative C−H bond activation is a fundamental process in Nature, mediated mainly by heme and nonheme enzymes, which employ high-valent iron−oxo complexes to perform selective C−H bond activation.[1,2] Identification of these elusive intermediates is still a formidable challenge in enzymatic bioinorganic chemistry.[1d,2a,b] For example, only recently was the long-postulated oxo−iron(IV)−porphyrin cation radical in P450 (Cpd I) identified and established in a working P450 enzyme.[2b] On the other hand, still awaiting direct observation is the corresponding oxo−iron(V) perferryl species postulated for nonheme Rieske oxygenases,[2c] which catalyze the unusual *cis*-dihydroxylation of arene C=C bonds as well as the hydroxylation of C−H bonds. Within the past decade, the chemistry of the Rieske oxygenases has inspired synthetic chemists to design and develop nonheme iron complexes that can activate H_2O_2 and catalyze the hydroxylation, epoxidation, or *cis*-dihydroxylation of hydrocarbon substrates with high stereoselectivity.[3a] On the basis of isotope labeling experiments that demonstrate incorporation of isotopes from $H_2{}^{18}O_2$ and $H_2{}^{18}$● into the oxidation products, Que and co-workers have proposed a so-called "water-assisted" mechanism that involves the coordination of water at a cis site of an observed low-spin Fe^{III}−OOH intermediate and the facilitation by water of O−O bond heterolysis to form an O=Fe^{V}−●H oxidant.[3b,c] Direct spectroscopic evidence for this putative iron(V) oxidant is scarce, but mass spectral evidence for an O=Fe^{V}−●H species was recently reported for one of these nonheme iron catalysts.[3d] DFT calculations have also shown that the formation of the postulated O=Fe^{V}−●H oxidant via the "water-assisted" mechanism was energetically feasible, with an activation barrier of 19.2−19.8 kcal/mol,[4a,b] and the ground

Received: February 20, 2013
Revised: April 19, 2013
Published: April 29, 2013

 © 2013 American Chemical Society

state for the Fe^{V} center was predicted to be $S = 3/2$.[4a,c] In this study, we focus on the chemistry of this family of nonheme iron catalysts with H_2O_2 as the oxidizing agent in the presence of acetic acid (AcOH), for which an $O{=}Fe^{V}{-}OAc$ oxidant is postulated, analogous to the $O{=}Fe^{V}{-}\bullet H$ oxidant in the absence of acetic acid.[5] Interestingly, our DFT results favor alternative electronic formulations of this species that are lower in energy than the perferryl electromer.

The "magic" of the AcOH additive in nonheme iron-catalyzed oxidations was first reported by White et al.,[6a] who showed that the presence of AcOH affected the reactivity and product distributions of these nonheme iron/H_2O_2 systems. Subsequently, the White group[6b−d] identified a synthetic nonheme complex, Fe(*S*,*S*-PDP) (see Scheme 1), that exhibited

Scheme 1. Systems Studied[a]

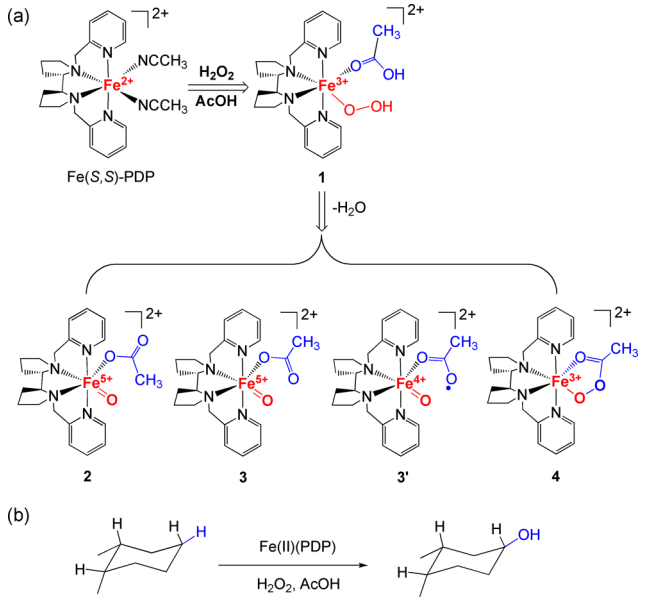

[a](a) A schematic representation of the putative oxidants **2**−**4** and their formation from Fe(*S*,*S*-PDP) with H_2O_2 in the presence of acetic acid. (b) The hydroxylation of *cis*-1,2-dimethylcyclohexane (*cis*-1,2-DMC) by these oxidants.

a controllable and efficient selectivity for the activation of tertiary and secondary C−H bonds in a variety of polyfunctional molecules, with the addition of AcOH being critical for the desired catalytic activity.[6b] Furthermore, White et al. showed[6a−c] that the mechanism follows the classical rebound mechanism,[1c] involving H-abstraction followed by rebound of an extremely short-lived substrate radical, but did not address the precise identity of the active species, which in the presence of AcOH gave such a robust catalytic system.

On the basis of parallel mechanistic work on related tetradentate ligand complexes,[5] Que et al. proposed that AcOH coordination to the hydroperoxoiron(III) intermediate forms **1**, which in turn leads to the generation of a perferryl $Fe^{V}{=}O$ oxidant **2** or **3** via a "carboxylic acid-assisted" mechanism (see Scheme 1).[5a] Talsi and co-workers used EPR to identify a new $S = 1/2$ signal with *g* values of 2.7, 2.4, and 1.5 that was generated by the combination of iron catalyst, H_2O_2, and acetic acid.[7] This novel EPR signature was attributed to **2**, and its decay was observed to be accelerated upon addition of cyclohexene with concomitant formation of the corresponding epoxide. However, its ultrashort lifetime allowed the new species to be generated in only about 10% yield, making it difficult to determine in detail the electronic properties of the high-valent iron center of this putative oxoperferryl oxidant. Such a description constitutes the main goal of this manuscript.

However, the $S = 1/2$ species observed by Talsi[7] has a spin state that does not correspond to the quartet ($S = 3/2$) ground state earlier calculated for the analogous $O{=}Fe^{V}{-}OH$ perferryl species.[4a,c] To clarify this puzzling situation, we have carried out further density functional theoretic (DFT) investigations of the oxoperferryl oxidants,[5,6] presumed to be formed in the presence of acetic acid from its hydroperoxo precursor (**1** in Scheme 1), and elucidated the mechanism for the hydroxylation of *cis*-1,2-dimethylcyclohexane (*cis*-1,2-DMC) reported by White et al.[6c] As we shall demonstrate, **2** is too high on the potential energy surface to be generated from **1**. Instead, what is formed is a 3-type species, but it has an electronic structure that is more suitably described as an $O{=}Fe^{IV}{-}AcO\cdot$ species and is labeled in Scheme 1a as **3′**. We find that **3′** has a very small barrier to collapse to a cyclic ferric peracetate complex (**4**), so **4** is the more likely species that is generated in the reaction. In the course of C−H activation, **4** serves as the precursor to an in situ $O{=}Fe^{IV}{-}AcO\cdot$ radical species that is generated along the reaction coordinate and effects C−H hydroxylation. The predictions regarding the nature of the oxidant formed in the presence of the AcOH additive are in line with known experimental data.

METHODS

The coordinates of Fe(S,S-PDP) was obtained from the Cambridge Crystallographic Data Centre[8] with the deposition number CCDC-661933, and cis-1,2-dimethylcyclohexane (cis-1,2-DMC) was employed as the substrate in the mechanistic study of methylene C−H bond activation at the equatorial position. DFT calculations were performed with the Gaussian 09 suite of quantum chemical packages.[9] The spin-unrestricted B3LYP functional[10] corrected with Grimme 06's dispersion[11] (denoted as UB3LYP-D2) was employed with two basis sets: (a) The TZVP basis set[12a,b] for iron, electron-rich N, and O atoms, and 6-31G** basis set for the rest C and H atoms. This basis set is denoted as B1 and is used to optimize transition states and minima. (b) The Def2-TZVPP basis set[12c] for all atoms, denoted as B2, and used for single-point energy corrections. Transition states were ascertained by vibrational frequency analysis to possess a single mode along the reaction path with only one imaginary frequency. All optimizations and single-point calculations were performed with solvation included using the self-consistent reaction field (SCRF) calculations, in the polarizable continuum model (PCM);[13] the experimental solvent acetonitrile ($\varepsilon = 35.688$) was used. The validation of DFT-D2 (with Grimme 06's dispersion correction) and the PCM model was assessed by DFT-D3(BJ)[14] (with Grimme's 2011 dispersion correction) and the SMD model (see Supporting Information Table S7). Further tests of species **2**−**4** were made with the five other functionals (B3P86-D2, B3PW91-D2, PBE0-D2, TPSSh-D2, and the double hybrid one B2PLYP-D2). All the functionals give the same ordering of these species. The mechanism of C−H hydroxylation was ascertained by intrinsic reaction coordinate following (IRC). The many computational details are presented in the Supporting Information (SI) document; here, we follow with the key results.

The kinetic isotope effect (KIE) for the O−O breaking process (using AcOH and AcOD) was determined using the

dx.doi.org/10.1021/cs400134g | ACS Catal. 2013, 3, 1334−1341

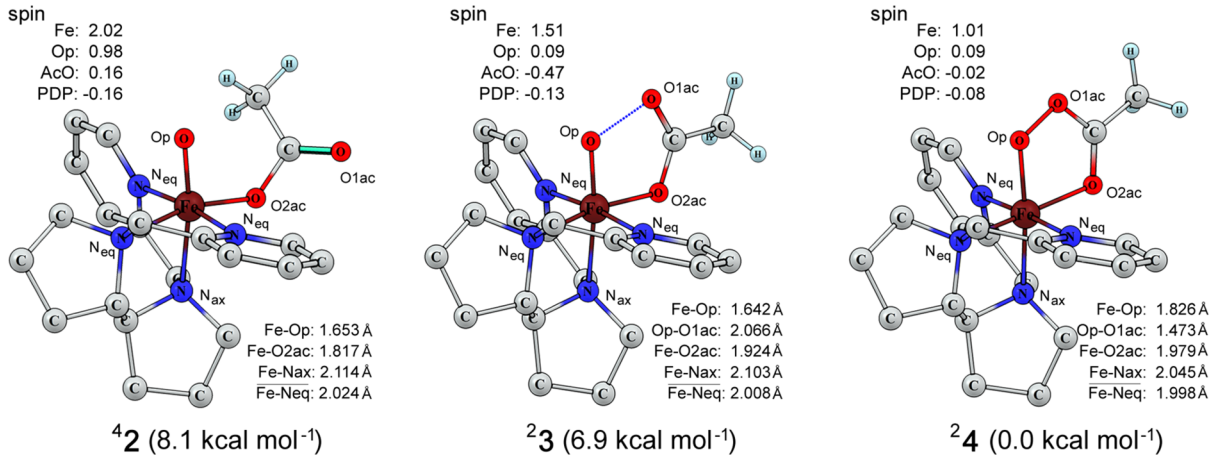

Figure 1. UB3LYP-D2/B1 geometries and spin densities of **2**−**4** in their lowest spin states. Relative energies are given at the UB3LYP-D2/B2//B1 computational level (including ZPE and solvation corrections). Hydrogen atoms on the PDP skeleton are omitted for clarity.

Gaussian frequency data based on the semiclassical Eyring equation. The KIE is given as

$$\left(\frac{k_H}{k_D}\right)_S = \exp\left[-\frac{(G_H^{\#} - G_H^R) - (G_D^{\#} - G_D^R)}{RT}\right]$$

where k denotes the reaction rate constant, G is the Gibbs free energy of activation, R is the gas constant, and T is the absolute temperature. As denoted by the subscript s, the so calculated KIE is semiclassical.

RESULTS AND DISCUSSION

Potential Active Oxidants. As previously proposed[5a,d] and shown in Scheme 1, the initial step involves formation of a solvated iron(III)−hydroperoxo complex, followed by ligand exchange of the CH_3CN solvent by AcOH to yield complex **1**. Subsequent loss of H_2O from **1** can generate the ultimate oxidant. Following this reaction sequence, we located three oxidants, **2**−**4**, with ground states that are shown in Figure 1.

Inspection of Figure 1 reveals that oxidants **3** and **4** have doublet (S = 1/2) spin ground states (see also Table S1 in the SI), and **2** has a quartet S = 3/2 state. Structurally, ^{4}**2** and ^{2}**3** are rotamers of each other, such that the C═O group of the acetate in **2** is in a gauche relationship to the Fe═O moiety, whereas in **3**, this relationship is syn. An additional electromer of **2** was also located; it has a doublet ground state, but it is 10.7 kcal mol^{-1} higher in energy than the quartet spin rotamer in Figure 1 (see Figure S3, SI). From a comparison of the relative energies and spin/geometric information for the ground spin states of **2**−**4**, it is apparent that the cyclic isomer ^{2}**4** is the most stable species, with ^{2}**3** and ^{4}**2** lying higher in energy, by 6.9 and 8.1 kcal mol^{-1}, respectively.

As the Figure reveals, the Fe═O moiety of ^{4}**2** has a spin density of ∼3 and the AcO ligand has only a small spin density. By contrast, ^{2}**3** has a significant spin density on both the Fe═O moiety and the AcO ligand, whereas ^{2}**4** possesses a spin density of unity on iron and a negligible spin elsewhere. To better elucidate the oxidation states and electronic structures of these oxidants, we show in Figure 2 the spin natural orbitals (SNOs).

Inspection of Figure 2a shows that ^{4}**2** possesses three singly occupied d-type orbitals. By analogy to O═Fe^V−OH,[4a,c] which has the same electronic structure, ^{4}**2** corresponds to a O═Fe^V−OAc perferryl species. The syn rotamer, ^{2}**3**, on the other hand, has an electronic structure with a filled δ_{xy} orbital

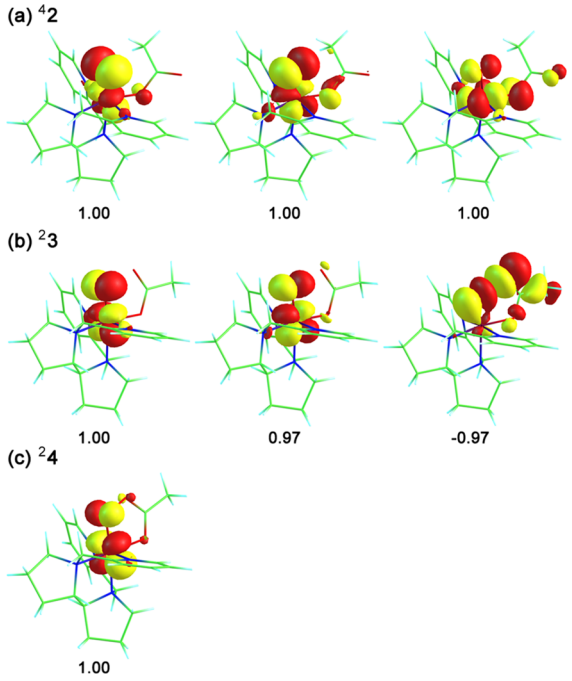

Figure 2. SNOs and their occupation numbers for (a) ^{4}**2**, (b) ^{2}**3**, and (c) ^{2}**4**. A negative occupation number corresponds to spin β. Doubly occupied d orbitals are not shown.

(not shown) and two singly occupied $\pi^*_{xz/yz}$ orbitals, and a fifth electron with spin β resides in a σ^*_{OpOac} orbital, which spans over the oxo ligand (O_p) and the oxygen atom of the acetate (O_{ac}). A large spin density is thus found on the OAc ligand, so ^{2}**3** is, in fact, better described as an O═Fe^{IV}−AcO· radical species, labeled in Scheme 1 as **3′**. By contrast, ^{2}**4** is a typical low-spin ferric complex with two filled d orbitals (not shown) and a singly occupied π^*_{yz} orbital. In summary, the presumed high-valent perferryl-oxo oxidant ^{4}**2** is the highest lying species, and its lower energy rotamer ^{2}**3′** is actually best described as O═Fe^{IV}−AcO· radical species, like Cpd I of P450.[2a,b] Both isomers lie well above the cyclic ferric peracetate ^{2}**4**. The S = 1/2 ground states of **3** and **4** are in line with Talsi's EPR data.[7] As such, in this respect, the DFT results match a spectroscopic characterization of the putative oxidant.

dx.doi.org/10.1021/cs400134g | ACS Catal. 2013, 3, 1334−1341

B. The Formation Mechanism of the Active Oxidants. To further examine the relationship of the cyclic ferric-peracetate **4** to the other oxidants, we present in Figure 3 the

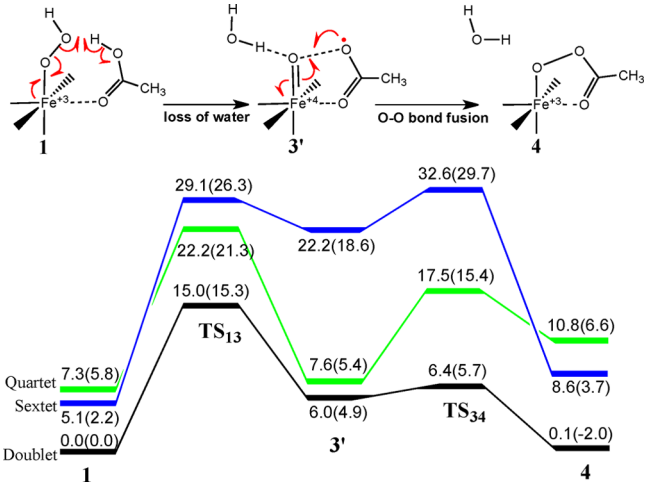

Figure 3. Energy profiles (in kcal mol^{-1}) for the transformation of hydroperoxo **1** to ferric peracetate **4** via **3′**. Values in parentheses are free energies. Outside the parentheses we show the UB3LYP-D2/B2//B1 SCF energies (including ZPE and solvation corrections).

computed transformation route from the hydroperoxo precursor **1** to **4**. Complex **1** has a doublet (S = 1/2) ground state, which is consistent with EPR data[5a] and previous theoretical results for $Fe^{III}(OOH)(H_2O)$.[4a] The rate-limiting step involves loss of H_2O by homolysis of the O−OH bond coupled to hydrogen transfer from AcOH. The calculated kinetic isotope effect for AcOH/AcOD is 3.3 (Table S11 in the SI). Cleavage of the O−OH bond leads to the formation of *syn*-oxoiron species **3** in various spin states, among which ^{2}**3′** is the oxoiron(IV)−AcO· radical species shown above in Scheme 1. The lowest transition state is ^{2}**TS$_{13}$** leading to ^{2}**3′** with an activation energy of 15.0 kcal mol^{-1}; the other TSs are much higher in energy. Subsequently, as shown in Figure 3, ^{2}**3′** undergoes O−O bond coupling (oxygen atoms of FeO and OAc) via ^{2}**TS$_{34}$**, with a tiny barrier of 0.4 (0.8) kcal mol^{-1}, and generates the cyclic ferric peracetate complex ^{2}**4**. Consequently, during transformation of the hydroperoxo precursor **1** to ^{2}**4**, the *syn*-oxoiron species ^{2}**3′** has a short lifetime. The rotational barrier of the AcO group in ^{2}**3′** to form the gauche-oxoiron oxidant ^{4}**2** is 1.2 kcal mol^{-1} higher and is spin-forbidden (Table S1 in the SI), whereas the spin-allowed process to ^{2}**2**, which lies 8.2 kcal mol^{-1} higher than ^{4}**2**, will encounter a barrier of at least 9.4 kcal mol^{-1}. Hence, ^{4,2}**2** will not be generated from ^{2}**3′** because the latter oxidant species falls in a virtually barrier-free fashion to form ^{2}**4**. As such, the only perferryl isomer, ^{4}**2**, which was identified here, cannot be a competent oxidant in the reaction.

On the other hand, ^{2}**3′** has some lifetime, albeit very short, and may, in principle, participate in oxidation of highly reactive substrates. Under most conditions, the only species that can accumulate during catalysis is ^{2}**4**. Thus, the theoretical results show clearly that the cyclic ferric-peracetate oxidant ^{2}**4** is the most likely oxidant candidate of the nonheme catalytic system in the presence of acetic acid. A similar cyclic intermediate to ^{2}**4** was considered previously and proposed to form by a mechanism involving nucleophilic attack of the hydroperoxo ligand on the bound carboxylate. In such a mechanism, both oxygen atoms of H_2O_2 would have been retained on the acylperoxo moiety, and one oxygen atom would end up on the acetate moiety upon O−O bond cleavage, but the latter was ruled out on the basis of an ^{18}O labeling experiment.[5a] This isotope labeling result, however, cannot rule out our proposed ^{2}**4** species, which incorporates only a single oxygen atom from the H_2O_2.

C. Hydroxylation of *cis*-1,2-DMC by 4. To establish the oxidative capability of this novel oxidant **4**, we studied the hydroxylation of a secondary C−H bond of *cis*-1,2-DMC mediated by **4**. Initially, one may consider H-abstraction by either O_{ac} or O_p. However, our calculations show that O_{ac} is not a good H abstractor, and the corresponding energy scan climbs significantly to 36 kcal/mol (see Figure S24 in the SI document). Thus, the reactive site must be O_p. As shown in Figure 4, the reaction initiated by H abstraction through O_p proceeds predominantly via the doublet state (S = 1/2), with a rather small activation energy barrier of 12.8 kcal mol^{-1} ($\Delta G^{\ddagger}$ = 12.3 kcal mol^{-1}). The reaction is effectively a concerted hydroxylation, albeit asynchronous (Figure S19 in the SI). Inspection of the geometric details of ^{2}**TS$_H$** demonstrates that it is a very "reagent-like" transition state, with a slightly stretched C−H bond (1.190 Å), a barely made H−O_p bond (1.458 Å), and an C···H···O_p angle of 160.5°. This "early" nature of the TS is in line with the relatively low energy barrier. We were not able to detect an intervening intermediate, and the reaction proceeds directly to the hydroxylated product. This hydroxylated product will be replaced by an H_2O_2 molecule, from which a proton transfer to the AcO ligand will regenerate the hydroperoxo complex **1** to initiate another cycle.

An interesting feature of the mechanism is displayed in Figure 4b−d. Inspection of the spin natural orbitals of ^{2}**TS$_H$** in Figure 3b shows that ^{2}**TS$_H$** is an oxoiron(IV) ferryl species, with two electrons in the π^* orbitals of the ferryl unit and a third electron delocalized in an orbital derived from the C−H and the O_p−O_{AcO} bonds. Clearly, as O−O homolysis begins in ^{2}**4** during the H abstraction, the oxidant is converted to an O═Fe^{IV}−AcO· radical species analogous to ^{2}**3′** (Figures 2b, c and S21−S22 in the SI). This is not an intermediate but, rather, a feature en-route to the TS, which we call pre-^{2}**TS$_H$** in Figure 3c, d. As shown in Figure 3d, the pre-^{2}**TS$_H$** feature has an oxoiron(IV) electron occupancy and one electron residing in the O−O antibonding orbital. As the C−H bond cleavage proceeds, a single electron shifts to the O−O antibonding orbital, leading to complete O−O cleavage and a ferryl unit. Indeed, ^{2}**TS$_H$** possesses a spin density of 1.6 on the Fe═O moiety, almost no spin on the AcO moiety, and a negative spin of −0.35 on the substrate moiety without the abstracted H. From the ^{2}**TS$_H$** downward, an additional electron shifts from the substrate "radical" moiety to the d block, thus leading to the ferric alcohol product complex, without an intervention of an intermediate. Thus, ^{2}**4** undergoes a preparatory electronic reorganization[15] and becomes a ferryl−acetoxyl radical species that abstracts the hydrogen atom from the substrate and leads to an effectively concerted hydroxylation. This intriguing mechanism was tested by following the intrinsic reaction coordinate (IRC), which showed that stepping forward from ^{2}**TS$_H$** indeed leads to the product complex, ^{2}**PC**. However, stepping down in the reverse direction does not lead directly to the ^{2}**4**-DMC cluster (^{2}**RC**). Instead, the IRC stops at a point, wherein the oxidant has the electronic structure of ^{2}**3′** (similar to the pre-**TS$_H$**), and which upon further geometry optimization converges to ^{2}**3′**, which we recall falls to ^{2}**4** in

dx.doi.org/10.1021/cs400134g | ACS Catal. 2013, 3, 1334−1341

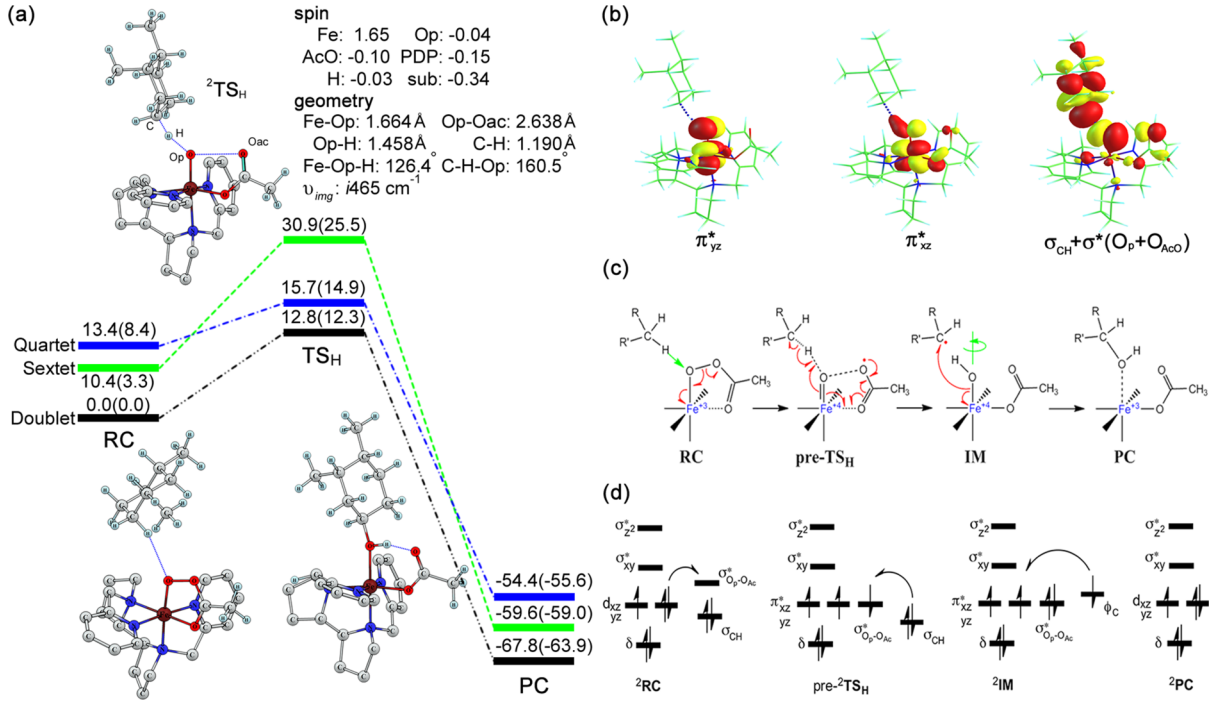

Figure 4. Mechanistic information on C−H hydroxylation of *cis*-1,2-DMC by **4**. (a) Energy profiles (kcal mol^{-1}) and geometries and spin densities of ^{2}**TS**$_{H}$. Values outside parentheses correspond to UB3LYP-D2/B2/B1 SCF energies (with ZPE and solvation correction). Inside parentheses are the corresponding UB3LYP-D2/B1 free energies (ZPE and solvation correction). Hydrogen atoms in the PDP skeleton are omitted for clarity. (b) The spin natural orbitals of ^{2}**TS**$_{H}$. (c) Schematic representation of the electron reorganization during the process. (d) Orbital occupation and electron-shift diagrams showing the electronic reorganization during the process. Note that pre-^{2}**TS**$_{H}$ and ^{2}**IM** are not real intermediates but features en-route to the TS, and from it, down to products.

virtually barrier-free fashion (Figure 3). Thus, starting from the ^{2}**4**-DMC cluster, in Figure 4, as the O−O cleavage progresses en route to ^{2}**TS**$_{H}$, the energy profile explores the region that electronically resembles ^{2}**3**′-DMC. This underscores the relative roles of ^{2}**4** and ^{2}**3**′; ^{2}**4** serves as the "bank" for generating a reactive ^{2}**3**′-like species that performs the substrate oxidation.

D. Comparison of Fe^{V}(O)(OAc) to Fe^{V}(O)(OH). An important question is what makes the acetate ligand so different from the OH ligand in the original O═Fe^{V}−OH oxidant?[4a,c] Why does it prevent the generation of a perferryl species, and why does it instead collapse to the cyclic structure ^{2}**4**? Inspection of the electronic distribution in ^{2}**3**′ (Figure 1) reveals that the closure to the cyclic structure is a simple coupling of two radical centers: one on the acetoxyl ligand and the other on the oxo moiety of Fe^{IV}═O. It should be noted that the original perferryl, O═Fe^{V}−OH, also has some O═Fe^{IV}−OH· character.[4a,c] However, the O−O coupling in HO−Fe^{V}═O would lead to the formation of an Fe^{III}(η^{2}-OOH) species. We tested the feasibility of this conversion, and the results are shown in Figure 5. In accord with previous calculations by Quiñonero et al.,[4b] it is seen from Figure 5 that the Fe^{III}(η^{2}-OOH) species is less stable than the O═Fe^{V}−OH species (11.8/13.8 kcal mol^{-1}), and it will therefore also have a high formation barrier due to the strain of forming a three-membered ring compared with the strain-free five-membered ring in ^{2}**4**.

E. Discussion of Experimental Data in Light of the DFT Results. The mechanistic insights from the DFT calculations described above can be used to understand the reactivity patterns previously observed for the various members of this nonheme iron catalyst family upon treatment with H_2O_2 and a carboxylic acid. The formation of species **1** in Scheme 1 was originally postulated on the basis of the change in the rhombic S = 1/2 EPR signal (g = 2.19, 2.15, 1.97) associated with the Fe^{III}−OOH intermediate to a more axial signal (g = 2.15, 2.15, 1.97) upon introduction of acetic acid.[5a] This spectral change suggested displacement of the solvent-derived ligand by AcOH. Moreover, the decay of **1** at −30 °C was found to be accelerated by the addition of AcOH, and the saturation behavior of this accelerative effect at around 0.1 M was consistent with a pre-equilibrium binding of AcOH to the iron(III) center, as suggested in Scheme 1. The rate of this decay showed a KIE of 2 when AcOD was used in place of AcOH, a value comparable to those obtained for other peroxoiron(III) systems undergoing O−O bond cleavage to form high-valent species.[16]

There is, in fact, experimental evidence consistent with the involvement of **3**′ in the reaction mechanism studied for the [Fe(TPA)] catalyst. It has been observed at −30 °C that the decay of **1** in the presence of a carboxylic acid afforded [Fe^{IV}(O)(TPA)]$^{2+}$,[5a] implying the cleavage of the O−O bond of the hydroperoxo ligand on **1** to oxidize the iron(III) center to the iron(IV) state. A reasonable place for the other oxidizing equivalent to reside is on a carboxyl radical. Indeed, when phenylacetic acid was used in place of AcOH in the above reaction, benzaldehyde was obtained as a stoichiometric byproduct. Benzaldehyde was proposed to derive from the aerobic oxidation of benzyl radical, which in turn would readily result from the loss of CO_2 from a transient phenylacetoxyl radical that would be formed when **1** decayed upon addition of phenylacetic acid. Moreover, the formation of benzaldehyde was found to be in competition with catalytic olefin epoxidation. Less benzaldehyde was produced when either a

dx.doi.org/10.1021/cs400134g | ACS Catal. 2013, 3, 1334−1341

higher concentration of olefin was present or a more electron-rich olefin was used as substrate. These results strongly suggest a common intermediate, i.e., **3′** or **4** (that becomes **3′** en route), that gives rise to both outcomes. A similar conclusion was reached in experiments with pentafluorobenzoic and related benzoic acids in place of acetic acid.[5c,d] These benzoic acids were found to undergo ipso hydroxylation, which would require decarboxylation of the starting benzoic acid via a mechanism similar to the phenylacetic acid mechanism. Ipso hydroxylation was also found to be competitive with catalytic olefin oxidation, strongly implicating a common oxidant for both transformations.[5d] On the basis of these observations, it was proposed that this common intermediate was an $[(L)Fe^{V}(O)(O_2CR)]^{2+}$ species (corresponding to **3** in Scheme 1), derived from heterolytic cleavage of the O−O bond of **1** that is promoted by the carboxylic acid, by analogy to the water-assisted pathway that affords the $[(L)Fe^{V}(O)(OH)]^{2+}$ oxidant in the absence of water. Subsequent internal electron transfer would then result in the formation of electromer **3′**.

An important new insight provided by the DFT calculations presented herein is that the carboxylic-acid-assisted pathway leading to the formation of an O═Fe^{V}−OAc perferryl oxidant **2** has a much higher barrier than the corresponding water-assisted pathway. Given this high barrier, we found an alternative pathway that results in facile O−O bond cleavage, leading to the formation of **4** via **3′** (Figure 3). Some experimental evidence for the involvement of a species such as **4** has been reported,[5b] which was based on the observation that the same olefin oxidation products and yields were observed when Fe(TPA) was treated with either peracetic acid or the combination of H_2O_2 and AcOH, but this observation has not been followed up in subsequent work.

There is, in fact, a synthetic precedent for a species such as **4**. Suzuki and co-workers reported the crystal structure of $[Fe^{III}L_2(\kappa^2\text{-}OOCO_2)]^{-}$ (L = quinoline-2-carboxylate), which was synthesized from the reaction of CO_2 with $[Fe^{III}L_2(\eta^2\text{-}O_2)]^{-}$.[17] The structure shows that the peroxocarbonate ligand forms a five-membered chelate ring with the iron, as calculated for **4**. One difference between this complex and **4** is that the iron(III) center of the Suzuki complex is high-spin, a feature that may provide it with the greater stability required for its crystallization.

Of significant relevance to this discussion are the results reported by Talsi for several members of the nonheme iron catalyst family.[7] They observed a new EPR signal with *g* values at 2.7, 2.4, and 1.5 when the iron catalyst was mixed with H_2O_2 and AcOH or was treated with peracid. This signal decayed more rapidly upon addition of cyclohexene, which was oxidized to the corresponding epoxide, implicating the EPR-active species as the oxidant. The *g* values of this EPR signal indicate an $S = 1/2$ system, which they assign to the $[(L)Fe^{V}(O)(O_2CR)]^{2+}$ oxidant. However, this signal strongly resembles features associated with a low-spin Fe(III) center. Because this novel EPR signal can be generated at present in only ∼10% yield, it is difficult to characterize by another spectroscopic method that can establish the iron oxidation state. The DFT results presented in this paper argue against the assignment of the oxidant as $[(L)Fe^{V}(O)(O_2CR)]^{2+}$ on the basis of both the high barrier (21.3 kcal mol^{-1}, including spin forbiddeness from the ground state, see Figure 3) found for its formation and the fact that it is calculated to have an $S = 3/2$ spin state, like the related the $[(L)Fe^{V}(O)(OH)]^{2+}$ oxidant. On the other hand, the EPR signal Talsi associates with the oxidant[7] is fully consistent with **4**, which is calculated to have an $S = 1/2$ spin state.

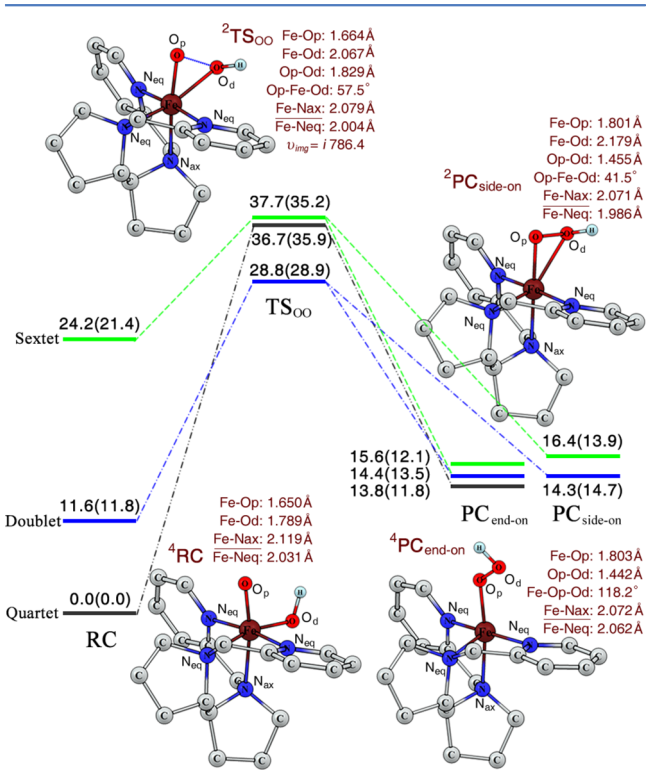

Figure 5. Energy profiles (kcal mol^{-1}) for the O═Fe^{V}−OH → Fe^{III}(OOH) transformation and geometries of the key intermediates on the ground state. Values outside parentheses correspond to UB3LYP-D2/B2/B1 SCF energies (with ZPE and solvation correction). Inside parentheses are the corresponding UB3LYP-D2/B1 free energies (ZPE and solvation correction). Hydrogen atoms in the PDP skeleton are omitted for clarity.

CONCLUSIONS

In summary, density functional calculations were performed to investigate the nature of the elusive oxidant in nonheme iron/H_2O_2/AcOH catalytic systems and its mechanism of formation. The theoretical results reveal that the long-presumed high-valent perferryl−oxo oxidant **2** is high in energy, whereas the lower energy-**3′** is better described as an oxoiron(IV)−AcO· radical species, with an electronic structure similar to that of Cpd I of P450, in the sense that in both cases, there is a noninnocent ligand that participates in the high valency. However, both the **2** and **3′** species are higher in energy compared with **4** and cannot accumulate during catalysis. Instead, what can build up during catalysis is the cyclic ferric peracetate complex ^{2}**4** (Scheme 1), which we propose to be the $S = 1/2$ EPR species experimentally observed by Talsi.[7] In the course of C−H bond activation, as the O−O bond cleaves, ^{2}**4** is converted to a transient oxoiron(IV)−AcO· species (similar to **3′**) that performs efficient C−H hydroxylation of alkanes. Thus, in the presence of acetic acid, the (*S*,*S*-PDP)Fe^{II}/H_2O_2 catalyst does not yield a perferryl complex analogous to O═Fe^{V}−OH, but nonetheless creates a potent oxidant that carries out concerted asynchronous C−H hydroxylation. These mechanistic findings provide insights into the influence of an additive such as acetic acid on catalysis by nonheme iron/H_2O_2 systems, including other iron complexes with a ligand sphere that has

dx.doi.org/10.1021/cs400134g | *ACS Catal.* 2013, 3, 1334−1341

two available cis coordination sites.[4b,c,5] The noninnocence of the additive completely alters the nature of the oxidant and further underscores the rich multioxidant scenario in the mechanistic landscape of these nonheme iron catalysts.[18]

■ ASSOCIATED CONTENT

Supporting Information

Twenty-four figures and 15 tables are presented to describe the mechanistic details. Cartesian coordinates of all involved complexes are also presented. This material is available free of charge via the Internet at http://pubs.acs.org.

■ AUTHOR INFORMATION

Corresponding Author

*E-mails: (Y.W.) wangyong@dicp.ac.cn, (L.Q.) larryque@umn.edu, (S.S.) sason@yfaat.ch.huji.ac.il.

Author Contributions

Calculations were done in Dalian and in Jerusalem. The manuscript was written through contributions of all authors. All authors have given approval to the final version of the manuscript.

Notes

The authors declare no competing financial interest.

■ ACKNOWLEDGMENTS

The work at DICP is supported by NFSC (Grant No. 21003116, 21173211 and 21233008) and by SKLMRD. The research at the HU is supported by the Israel Science Foundation. L.Q. acknowledges the US Department of Energy, Office of Basic Energy Sciences (Grant No. DE-FG02-03ER15455) for support.

■ REFERENCES

(1) (a) Sono, M.; Roach, M. P.; Coulter, E. D.; Dawson, J. H. *Chem. Rev.* **1996**, *96*, 2841−2887. (b) Costas, M.; Mehn, M. P.; Jensen, M. P.; Que, L., Jr. *Chem. Rev.* **2004**, *104*, 939−986. (c) Groves, J. T. *J. Chem. Educ.* **1985**, *62*, 928−931. (d) Krebs, C.; Fujimori, D. G.; Walsh, C. T.; Bollinger, J. M., Jr. *Acc. Chem. Res.* **2007**, *40*, 484−492. (e) Que, L., Jr. *Acc. Chem. Res.* **2007**, *40*, 493−500. (f) Nam, W. *Acc. Chem. Res.* **2007**, *40*, 522−531.

(2) (a) Schlichting, I.; Berendzen, J.; Chu, K.; Stock, A. M.; Maves, S. A.; Benson, D. E.; Sweet, R. M.; Ringe, D.; Petsko, G. A.; Sligar, S. G. *Science* **2000**, *287*, 1615−1622. (b) Rittle, J.; Green, M. T. *Science* **2010**, *330*, 933−937. (c) Chakrabarty, S.; Austin, R. N.; Deng, D.; Groves, J. T.; Lipscomb, J. D. *J. Am. Chem. Soc.* **2007**, *129*, 3514−3515.

(3) (a) Que, L., Jr.; Tolman, W. B. *Nature* **2008**, *455*, 333−340. (b) Chen, K.; Que, L., Jr. *J. Am. Chem. Soc.* **2001**, *123*, 6327−6337. (c) Chen, K.; Costas, M.; Kim, J.; Tipton, A. K.; Que, L., Jr. *J. Am. Chem. Soc.* **2002**, *124*, 3026−3035. (d) Prat, I.; Mathieson, J. S.; Güell, M.; Ribas, X.; Luis, J. M.; Cronin, L.; Costas, M. *Nat. Chem.* **2011**, *3*, 788−793.

(4) (a) Bassan, A.; Blomberg, M. R. A.; Siegbahn, P. E. M.; Que, L., Jr. *J. Am. Chem. Soc.* **2002**, *124*, 11056−11063. (b) Quiñonero, D.; Morokuma, K.; Musaev, D. G.; Mas-Balleste, R.; Que, L., Jr. *J. Am. Chem. Soc.* **2005**, *127*, 6548−6549. (c) Chen, H.; Lai, W. Z.; Yao, J. N.; Shaik, S. *J. Chem. Theory Comput.* **2011**, *7*, 3049−3052.

(5) (a) Mas-Balleste, R.; Que, L., Jr. *J. Am. Chem. Soc.* **2007**, *129*, 15964−15972. (b) Fujita, M.; Que, L., Jr. *Adv. Synth. Cat.* **2004**, *346*, 190−194. (c) Makhlynets, O. V.; Das, P.; Taktak, S.; Flook, M.; Mas-Balleste, R.; Rybak-Akimova, E. V.; Que, L., Jr. *Chem.—Eur. J.* **2009**, *15*, 13171−13180. (d) Das, P.; Que, L., Jr. *Inorg. Chem.* **2010**, *49*, 9479−9485.

(6) (a) White, M. C.; Doyle, A. G.; Jacobsen, E. N. *J. Am. Chem. Soc.* **2001**, *123*, 7194−7195. (b) Chen, M. S.; White, M. C. *Science* **2007**, *318*, 783−787. (c) Chen, M. S.; White, M. C. *Science* **2010**, *327*, 566−571. (d) White, M. C. *Science* **2012**, *335*, 807−809.

(7) (a) Lyakin, O. Y.; Bryliakov, K. P.; Britovsek, G. J. P.; Talsi, E. P. *J. Am. Chem. Soc.* **2009**, *131*, 10798−10799. (b) Lyakin, O. Y.; Bryliakov, K. P.; Talsi, E. P. *Inorg. Chem.* **2011**, *50*, 5526−5538. (c) Lyakin, O. Y.; Ottenbacher, R. V.; Bryliakov, K. P.; Talsi, E. P. *ACS Catal.* **2012**, *2*, 1196−1202.

(8) These data can be obtained free of charge from The Cambridge Crystallographic Data Centre via www.ccdc.cam.ac.uk/data_request/cif.

(9) Frisch, M. J.; Trucks, G. W.; Schlegel, H. B.; Scuseria, G. E.; Robb, M. A.; Cheeseman, J. R.; Scalmani, G.; Barone, V.; Mennucci, B.; Petersson, G. A.; Nakatsuji, H.; Caricato, M.; Li, X.; Hratchian, H. P.; Izmaylov, A. F.; Bloino, J.; Zheng, G.; Sonnenberg, J. L.; Hada, M.; Ehara, M.; Toyota, K.; Fukuda, R.; Hasegawa, J.; Ishida, M.; Nakajima, T.; Honda, Y.; Kitao, O.; Nakai, H.; Vreven, T.; Montgomery, J. A., Jr.; Peralta, J. E.; Ogliaro, F.; Bearpark, M.; Heyd, J. J.; Brothers, E.; Kudin, K. N.; Staroverov, V. N.; Kobayashi, R.; Normand, J.; Raghavachari, K.; Rendell, A.; Burant, J. C.; Iyengar, S. S; Tomasi, J.; Cossi, M.; Rega, N.; Millam, J. M.; Klene, M.; Knox, J. E.; Cross, J. B.; Bakken, V.; Adamo, C.; Jaramillo, J.; Gomperts, R.; Stratmann, R. E.; Yazyev, O.; Austin, A. J.; Cammi, R.; Pomelli, C.; Ochterski, J. W.; Martin, R. L.; Morokuma, K.; Zakrzewski, V. G.; Voth, G. A.; Salvador, P.; Dannenberg, J. J.; Dapprich, S.; Daniels, A. D.; Farkas, O.; Foresman, J. B.; Ortiz, J. V.; Cioslowski, J.; Fox, D. J. *Gaussian 09, revision C.01*; Gaussian, Inc.: Wallingford, CT, 2009.

(10) (a) Becke, A. D. *J. Chem. Phys.* **1992**, *96*, 2155−2160. (b) Becke, A. D. *J. Chem. Phys.* **1992**, *97*, 9173−9182. (c) Becke, A. D. *J. Chem. Phys.* **1993**, *98*, 5648−5652. (d) Lee, C.; Yang, W.; Parr, R. G. *Phys. Rev. B* **1988**, *37*, 785−789.

(11) Grimme, S. *J. Comput. Chem.* **2006**, *27*, 1787−1799.

(12) (a) Schaefer, A.; Horn, H.; Ahlrichs, R. *J. Chem. Phys.* **1992**, *97*, 2571−2577. (b) Schaefer, A.; Huber, C.; Ahlrichs, R. *J. Chem. Phys.* **1994**, *100*, 5829−5835. (c) Weigend, F.; Ahlrichs, R. *Phys. Chem. Chem. Phys.* **2005**, *7*, 3297−3305.

(13) Tomasi, J.; Mennucci, B.; Cammi, R. *Chem. Rev.* **2005**, *105*, 2999−3093.

(14) (a) Grimme, S.; Antony, J.; Ehrlich, S.; Krieg, H. *J. Chem. Phys.* **2010**, *132*, 154104−154119. (b) Grimme, S.; Ehrlich, S.; Goerigk, L. *J. Comput. Chem.* **2011**, *32*, 1456−1465.

(15) Ye, S.; Neese, F. *Proc. Natl. Acad. Sci. U.S.A.* **2011**, *108*, 1228−1233.

(16) (a) Dunford, H. B.; Hewson, W. D.; Steiner, H. *Can. J. Chem.* **1978**, *56*, 2844−2852. (b) Traylor, T. G.; Xu, F. *J. Am. Chem. Soc.* **1990**, *112*, 178−186. (c) Lee, S. K.; Lipscomb, J. D. *Biochemistry* **1999**, *38*, 4423−4432. (d) Tinberg, C. E.; Lippard, S. J. *Biochemistry* **2009**, *48*, 12145−12158.

(17) Hashimoto, K.; Nagatomo, S.; Fujinami, S.; Furutachi, H.; Ogo, S.; Suzuki, M.; Uehara, A.; Maeda, Y.; Watanabe, Y.; Kitagawa, T. *Angew. Chem., Int. Ed.* **2002**, *41*, 1202−1205.

(18) See a discussion forum in (a) Shaik, S.; de Visser, S. P.; Kumar, D. *J. Biol. Inorg. Chem.* **2004**, *9*, 661−668. (b) Que, L., Jr. *J. Biol. Inorg.Chem.* **2004**, *9*, 643−643. (c) Nam, W.; Ryu, Y. O.; Song, W. J. *J. Biol. Inorg. Chem.* **2004**, *9*, 654−660.

■ NOTE ADDED IN PROOF

While this paper was undergoing review and revision, a paper appeared in *J. Am. Chem. Soc.* **2013**, *135*, 4235−4249 by Ansari, Kaushik, and Rajaraman, which used DFT calculations to gain insight into the mechanism for *ortho*-hydroxylation of benzoic acids by the Fe(TPA)/H_2O_2 system, which is analogous to the Fe((*S,S*)-PDP)/H_2O_2 system discussed in this paper. In disagreement with our results, Ansari *et al.* reported calculations that favor $Fe^{V}O$(TPA)(OBz) as the oxidant responsible for the reaction. However our calculations, which were done with a higher level basis set (optimization with the TZVP(Fe, N, O)/6-31G**(C, H) basis set and single-point energy calculations with the Def2-TZVPP basis set), show that the most stable

electromer in the Fe(TPA) system is in fact analogous to ^{2}**4** and not the $Fe^{V}O(TPA)(OBz)$ species, as reported by Ansari *et al.*

dx.doi.org/10.1021/cs400134g | *ACS Catal.* 2013, 3, 1334−1341